Bjerknes Compensation in the CMIP5 Climate Models

STEPHEN OUTTEN AND IGOR ESAU

Nansen Environmental and Remote Sensing Center, Bjerknes Centre for Climate Research, Bergen, Norway

ODD HELGE OTTERÅ

Uni Research Climate, Bjerknes Centre for Climate Research, Bergen, Norway

(Manuscript received 7 February 2018, in final form 6 August 2018)

ABSTRACT

This study examines the atmospheric and oceanic heat transports in preindustrial control and historical runs of 15 fully coupled global climate models from the CMIP5 project. The presence of Bjerknes compensation is confirmed in all models by the strong anticorrelation and approximately equal magnitude of the anomalies of these heat transports. Previous studies of Bjerknes compensation in the absence of external forcing have all shown the strongest compensation at high latitudes, where the warm ocean meets the cold Arctic atmosphere. In this study, however, it is found that many of the 15 models have a second and often dominant peak of compensation in the northern midlatitudes, where strong air–sea interaction is often associated with the midlatitude storm tracks. It has also been suggested that variations in heat transport in the ocean lead those in the atmosphere, but this work has found no clear and robust support for this, as only half the models show such a relationship. In the historical simulations where external forcings are applied, Bjerknes compensation continues to be present, but many models show pronounced trends in the heat transports. All of the models show multidecadal variability in heat transports in both preindustrial control and historical simulations. Any anthropogenic climate change signal could potentially be masked or amplified by the natural variability governed by Bjerknes compensation. Given its presence in the CMIP5 models, which are the basis of so much policy and adaptation planning, an improved understanding of Bjerknes compensation may have socioeconomic relevance for the future.

1. Introduction

A critical component for maintaining Earth's climate is the meridional heat transport through the atmosphere and ocean. This transport allows heat to move from the tropics, where the heating is strongest, to the polar region, where longwave radiation to space allows the climate system to cool. Natural variability in the meridional heat transport occurs on all time scales, but understanding this variability on decadal to multidecadal time scales will provide insight into the predictability of Earth's climate system. A good understanding of the natural variability of the climate system is also essential for a more accurate attribution of natural and anthropogenic forcing factors to the observed climate change, though as stated in the Fifth Assessment Report (AR5) of the Intergovernmental Panel on Climate Change (IPCC), the industrial-era natural forcing is a small fraction of the anthropogenic forcing (Myhre et al. 2013).

Jacob Bjerknes proposed 50 years ago that large anomalies in heat transported by the atmosphere and ocean should approximately balance one another (Bjerknes 1964), a scenario now called Bjerknes compensation (BJC). BJC arises by assuming that the top-of-atmosphere fluxes and the ocean heat content are approximately constant, and therefore the total energy transported around the climate system must also be approximately constant. The presence of BJC in the climate system is difficult to accurately assess given the lack of comprehensive ocean heat content measurements; however, it

Denotes content that is immediately available upon publication as open access.

Supplemental information related to this paper is available at the Journals Online website: https://doi.org/10.1175/JCLI-D-18-0058.s1.

Corresponding author: Stephen Outten, stephen.outten@nersc.no

DOI: 10.1175/JCLI-D-18-0058.1

has been identified in a few climate models. BJC was first identified in the Hadley Centre Coupled Model, version 3 (HadCM3; Shaffrey and Sutton 2004, 2006). They showed that the connection between the surface heat fluxes and the oceanic energy transport was weakened on interannual time scales, since the heat budget of the upper ocean is strongly influenced by the variability in heat storage in the upper ocean. However, BJC was clearly identified at decadal time scales by the signature strong anticorrelation between the anomalies of atmospheric and ocean heat transport. More recently BJC has also been identified in ECHAM5/Max Planck Institute Ocean Model (MPIOM; Jungclaus and Koenigk 2010) and the Bergen Climate Model (BCM; Outten and Esau 2017), although the compensation was weaker in ECHAM5/MPIOM.

In all three models, the compensation was found to be strongest at high latitudes, peaking at around 70°N. At this latitude, the heat transport in the ocean is restricted mainly to the Atlantic sector. Shaffrey and Sutton (2006) suggested links between the variability of BJC and the Atlantic meridional overturning circulation (AMOC) in HadCM3. Jungclaus and Koenigk (2010) related the long-term changes of BJC to the pattern of large-scale flow, linking the compensation mechanism to an Arctic Oscillation–like pattern in sea level pressure. They suggested that the climate at high latitudes is modulated by the heat transport anomalies available, and that a drastic warming and cooling can only occur when the atmosphere and ocean act in concert, an idea shared by Held (2001).

Regressions of the heat transports at the latitude of maximum compensation have provided insights into the coupling mechanism between the atmosphere and ocean. At this high latitude, the increased heat transport occurring when BJC is in an ocean positive phase (i.e., during periods of positive ocean heat transport anomaly) is associated with decreased sea ice in the Greenland and Nordic Seas (Van der Swaluw et al. 2007; Outten and Esau 2017) and in the Barents Sea (Jungclaus and Koenigk 2010; Outten and Esau 2017). It has been demonstrated that this reduction in sea ice cover results in an increased sea–air heat flux that causes a decrease in the meridional temperature gradient in the atmosphere (Van der Swaluw et al. 2007), which is in turn associated with changes to the large-scale atmospheric flow (Jungclaus and Koenigk 2010; Outten and Esau 2017).

Yang et al. (2013) performed a coupled model sensitivity experiment to assess the response of meridional heat transports to freshening of the oceans in the Fast Ocean–Atmosphere Model (Jacob 1997). They found that increased freshwater into the Northern Hemisphere (NH) led to sea surface temperature (SST) cooling in the NH and SST warming in the Southern Hemisphere (SH). This, in turn, decreased northward heat transport in the ocean and led to increased heat transport in the atmosphere through an enhancement of the Hadley cell. Subsequent work by Yang et al. (2015a) decomposed the atmospheric and oceanic heat transport into individual components. They confirmed the presence of BJC through the strong anticorrelation of the atmospheric and oceanic heat transport anomalies but did not investigate this potential mechanism further in their study.

Other works have focused on investigating the mechanism underlying BJC through the use of less complex models (e.g., coupled box models; Yang et al. 2016). Liu et al. (2016) proposed a theory for the mechanism of BJC by employing an energy balance model to investigate the role of climate feedbacks in shaping BJC. They found that for a stable climate dominated by negative climate feedbacks, the anomalies in the atmospheric heat transport were always compensated for by the anomalies of oceanic heat transport. However, the strength of this compensation changed significantly if the climate feedbacks changed. In more complex climate models or in the real climate system, climate feedbacks, such as the sea ice albedo positive feedback in polar regions or the negative feedback between outgoing longwave flux and the surface temperature, are generally challenging to estimate and can vary dramatically in both time and space depending on the dynamical processes present. Therefore, as stated in Liu et al. (2016), further work is required to link this theory to complex climate models.

Farneti and Vallis (2013) investigated heat transports in GFDL CM2.1, but since the heat transports in that study were averaged over 20°–70°N, they found a weaker BJC than in previous works, and the signal for the latitude of strongest compensation could not be identified or compared to previous findings. Another study identified Bjerknes-like behavior in the North Pacific in the Community Earth System Model (CESM) but as the authors state, it was not a true BJC signal since it was limited to a local-scale balance (Bishop et al. 2015).

Although BJC has been identified previously in a few coupled climate models, there are still open questions of whether or not BJC is present in the wider range of climate models contained in phase 5 of the Coupled Model Intercomparison Project (CMIP5) and to what extent BJC will be present under varying external forcings, as found in the historical runs and future scenario simulations. Natural variability of global heat transport could mask or amplify anthropogenic climate change signals. Since much of the policy and adaptation planning for the future are based on CMIP5 scenarios, a better understanding of BJC in these models is of socioeconomic relevance.

TABLE 1. List of CMIP5 models used in this study, along with the respective modeling center or group that ran the models and prepared the output for the CMIP5 archive. The H_O derivation column refers to the method employed in this study to obtain the meridional ocean heat transport H_O. "Direct" indicates the CMIP5 archive included H_O in the field hfbasin, while "zigzag" indicates it was calculated from hfy and hfx, accounting for model grid (see section 2). The length in years of the preindustrial control run (piCtrl) is also given.

Modeling center	Country	Institute ID	Model name	H_O derivation	piCtrl length (yr)
Commonwealth Scientific and Industrial Research Organisation (CSIRO) and Bureau of Meteorology (BoM)	Australia	CSIRO-BOM	ACCESS1.0,	Direct	500
			ACCESS1.3	Direct	500
CSIRO in collaboration with Queensland Climate Change Centre of Excellence (QCCCE)	Australia	CSIRO-QCCCE	CSIRO Mk3.6.0	Direct	500
Centre National de Recherches Météorologiques (CNRM)/Centre Européen de Recherche et de Formation Avancée en Calcul Scientifique (CERFACS)	France	CNRM-CERFACS	CNRM-CM5	Zigzag	850
L'Institut Pierre-Simon Laplace (IPSL)	France	IPSL	IPSL-CM5A-MR	Zigzag	300
			IPSL-CM5B-LR		300
LASG, Institute of Atmospheric Physics (IAP), Chinese Academy of Sciences	China	LASG-IAP	FGOALS-s2	Direct	500
NOAA Geophysical Fluid Dynamics Laboratory (GFDL)	United States	NOAA GFDL	GFDL-ESM2G	Zigzag	500
			GFDL-ESM2M	Zigzag	500
NASA GISS	United States	NASA GISS	GISS-E2-R	Zigzag	550
			GISS-E2-R-CC	Zigzag	251
Institute of Numerical Mathematics (INM)	Russia	INM	INM-CM4.0	Direct	500
Meteorological Research Institute (MRI)	Japan	MRI	MRI-CGCM3	Direct	500
Norwegian Climate Centre	Norway	NCC	NorESM1-M	Direct	500
			NorESM1-ME	Direct	252

This work identifies BJC in a selection of preindustrial control and historical runs from CMIP5. It compares the findings to those from previous works and highlights the notable differences found. The data sources and calculations of BJC are explained in the next section. Section 3 provides an overview of BJC in the preindustrial control runs, while section 4 examines BJC in the historical runs. Discussion and conclusions are given in sections 5 and 6, respectively.

2. Data sources and analysis

The model data used in this work come from the preindustrial control and historical runs of 15 global, fully coupled, atmosphere–ocean–sea ice general circulation models from the CMIP5 archive. The names of the selected models along with the modeling groups that employed them are given in Table 1. This study included all models available in the CMIP5 archive on the Earth System Grid Federation (ESGF) platform that had the complete model field required to calculate both the atmospheric and oceanic heat transports needed for assessing BJC. Other models were examined but subsequently excluded because of them lacking one or more of the required model fields. These model fields were not the first priority in the CMIP5 experiment design protocol, therefore modeling groups were under no obligation to produce or output these fields, hence their absences for many models.

To assess the presence of BJC, the meridional heat transports in the atmosphere H_A and ocean H_O were obtained. For the atmosphere, this was calculated following the formulation of Shaffrey and Sutton (2006), using the integration of the divergence of the zonally integrated surface flux F_{sfc} and top-of-atmosphere (TOA) flux F_{toa}:

$$\frac{\partial H_A}{\partial y} = F_{\text{sfc}} - F_{\text{toa}}. \tag{1}$$

The H_O was obtained directly for 8 of the 15 models (Table 1) from the CMIP5 variable northward ocean heat transport (hfbasin). This contains the meridional heat transport separately for Atlantic–Arctic Ocean and the Pacific–Indian Ocean, as well as for the global ocean, which was used in this study. The hfbasin variable was unfortunately not available for the other seven models. For these seven models, H_O was calculated from the CMIP5 variables "ocean heat y transport" (hfy) and "ocean heat x transport" (hfx). The hfy and hfx variables provide the heat transports in the y and x directions of the model grid, which for the ocean is often in a dipole or tripole configuration with poles situated in

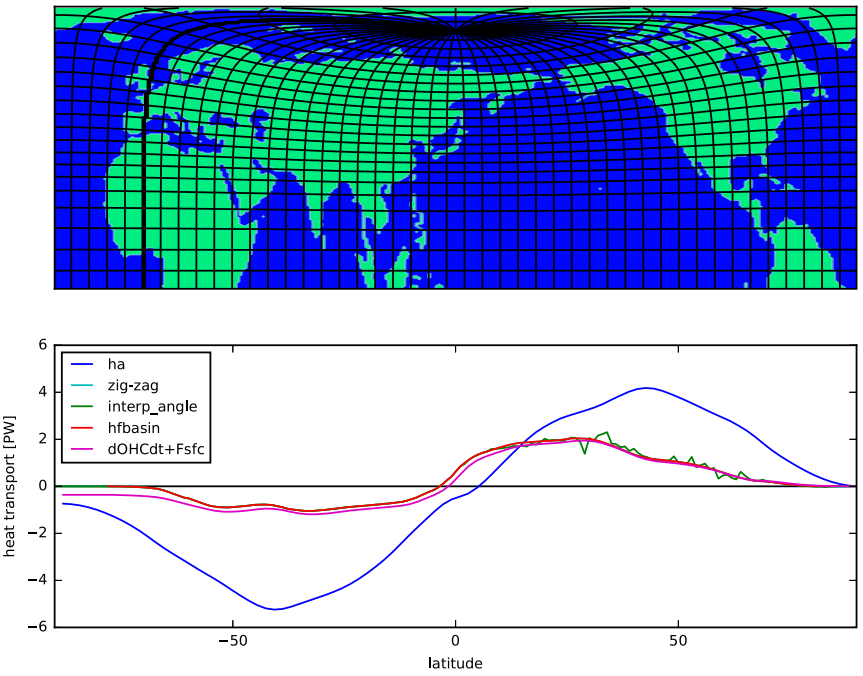

FIG. 1. (top) NorESM1-M ocean model grid with lines of latitude and longitude contoured. (bottom) Mean meridional heat transports (PW) as a function of latitude for the preindustrial control run of NorESM1-M for the atmosphere H_A (blue); ocean as directly output from the model, hfbasin (red); calculated from hfy and hfx using the grid angle interp_angle (green); calculated using the sum of surface flux and rate of change of ocean heat content (magenta); and calculated using the zigzag method employed in this work (cyan). The zigzag line is overlapped by hfbasin line.

the high-latitude NH [e.g., Norwegian Earth System Model, version 1 (NorESM1-M); Fig. 1]. This means that in the Southern Hemisphere and close to the equator, hfy is equivalent to the meridional heat transport. However, when moving northward, away from the equator, the grid becomes increasingly curved as it approaches the model grid poles and the true meridional heat transport becomes a partial combination of hfy and hfx. In the regions north of the model grid poles, the grid is so distorted that hfy effectively becomes a southward flow, so a negative partial value must be used to obtain the meridional transport. These factors make it difficult to calculate H_O in a straightforward and consistent manner across multiple models with different ocean grids.

Two methods were tested to accurately calculate H_O in the seven models for which hfbasin was not available. Since the output of the NorESM included both the hfbasin and hfy/hfx model variables, it was possible to validate the heat transports calculated with both of these methods against the heat transport directly output by the model (Fig. 1). For comparison, the method employed in previous studies of using a sum of net surface flux and rate of change of ocean heat content to calculate an "implied" meridional heat transport is also shown in Fig. 1. The first and most straightforward method was to convert hfy and hfx into northward and eastward components using the grid angle at each grid cell. While in principle this approach should produce an accurate meridional heat transport, small differences were found when compared to heat transport directly output from the model at all locations where the grid was curved. Investigation revealed that the grid angle is given for the p points of the grid cells (i.e., the center of each grid cell), while the hfy and hfx were given on the top and bottom and left and right edges of the grid cell, respectively, as per a standard C-grid configuration. Thus the angles given are not accurate for the locations of hfy and hfx, hence the small differences in the calculated heat transport when compared to the heat transport output directly from the model. The differences manifest themselves with sharp changes from one latitude to the next.

To resolve this problem and obtain an accurate calculation of H_O, a second method was employed, which is hereafter referred to as the zigzag method and is shown schematically in Fig. 2. In this method, grid cells are selected along a line of single latitude. A zonal boundary

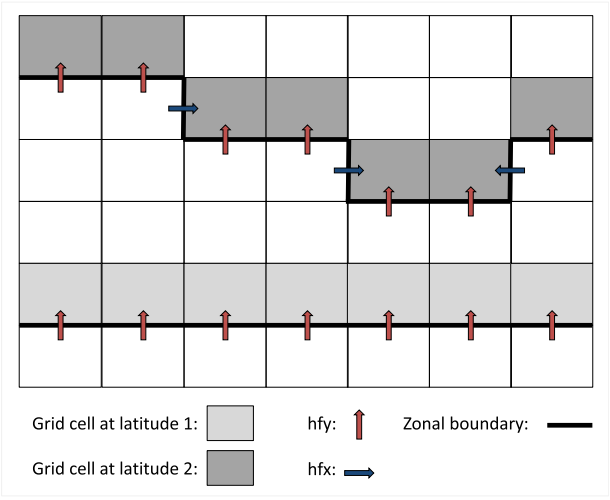

FIG. 2. Schematic of zigzag method for calculating meridional ocean heat transport H_O. Grid cells are identified at latitude 1, where there is no grid curvature. The boundary is identified and the heat flux is entirely composed of heat flux in the y direction (hfy), as expected. Latitude 2 is closer to a model grid pole, hence it experiences curvature, and grid cells at latitude 2 are not on the same row in the model grid. The boundary is identified, but this time the fluxes across this boundary include heat fluxes in both the y and x directions, some of which are negative (opposite direction).

is then identified from the edges of these grid cells, and the fluxes across this boundary are summed to give the meridional transport at the respective latitude. At latitudes where the model grid is not curved (Fig. 2, light gray boxes), identified grid cells are on a single model grid row, and the derived meridional heat flux is composed entirely of the ocean heat transport in the y direction. However, at latitudes closer to the model grid poles where the grid is curved, the identified cells at a single latitude are not on the same row, thus the transport across the boundary includes heat transport in both the y and x directions. Depending upon the direction in which the boundary is crossed, some of these values may be negative, for example, hfy that is southward transport due to extreme grid curvature. The process was repeated at each latitude to obtain a complete meridional ocean heat transport H_O. The benefit of the zigzag method is that it accurately reproduced the heat transport as directly output by the model, and it produced a smoother transition of heat flux from one latitude to the next (Fig. 1). ACCESS1.0, ACCESS1.3, and MRI-CGCM3 also included both hfbasin and hfy/hfx variables in their output. The zigzag method was tested using these models and found to produce the best estimate of the meridional ocean heat transport in all cases when compared to the values directly output from the models. Therefore, the zigzag method was used for the seven models for which hfbasin was not available (Table 1).

Monthly model output was used for all variables and an 11-yr running mean was applied to emphasize the multidecadal variability, per Shaffrey and Sutton (2006), Jungclaus and Koenigk (2010), and Outten and Esau (2017). To allow for a direct comparison at specific latitudes between the atmospheric and oceanic heat transports, H_A was interpolated to the latitudinal grid of H_O using a one-dimensional cubic interpolation.

3. BJC in CMIP5 preindustrial control runs

The total meridional heat transports in the atmosphere H_A and ocean H_O were calculated for the preindustrial control runs of the 15 CMIP5 models (Fig. S1 in the online supplemental material). The length of the preindustrial control runs varies from model to model, but most are 500 years long (Table 1). All of the models produce broadly similar structures of mean heat transports as a function of latitude, with maxima in heat transport in H_A located at approximately 40°N and 40°S, with a maximum in H_O located at around 20°N, and with a broader and less well-defined negative peak in H_O located between 20° and 40°S (e.g., NorESM1-M; Fig. 1). In the NH, the maxima in H_A are found between 4 and 5 PW (1 PW = 10^{15} W) in most of the models, with only IPSL-CM5B-LR outside of this range at 5.1 PW. This compares well to values found in previous model studies (Shaffrey and Sutton 2006; Jungclaus and Koenigk 2010; Outten and Esau 2017) and to estimates from the NCEP–NCAR and ECMWF reanalyses (Trenberth and Caron 2001), which varied between 3.8 (HadCM3) and 5.2 PW (NCEP–NCAR reanalyses). For the ocean, the maxima in H_O in the NH from previous studies were between 1.2 (ECHAM5 model) and 2.1 PW (NCEP–NCAR reanalyses). The NH H_O maxima were within this range for 11 of the CMIP5 models, with GFDL-ESM2G having slightly higher ocean heat transport peaking around 2.3 PW and IPSL-CM5B-LR, FGOALS-s2, and INM-CM4.0 having slightly lower ocean heat transport peaking just below 1 PW. These results suggest that all 15 CMIP5 models are producing reasonable estimates of both H_A and H_O in the NH compared to previous estimates from both models and reanalyses. These results also suggest that the greatest differences between the models are associated with the oceanic contribution to the meridional heat transport. This is in line with existing literature pointing to air–sea fluxes as a key source of uncertainty in climate models, with profound impact on ocean circulation and ocean heat uptake (Huber and Zanna 2017).

In the SH, the CMIP5 models show a negative peak in H_A between −4 and −6 PW, with the CNRM-CM5 and INM-CM4.0 having stronger atmospheric heat transport,

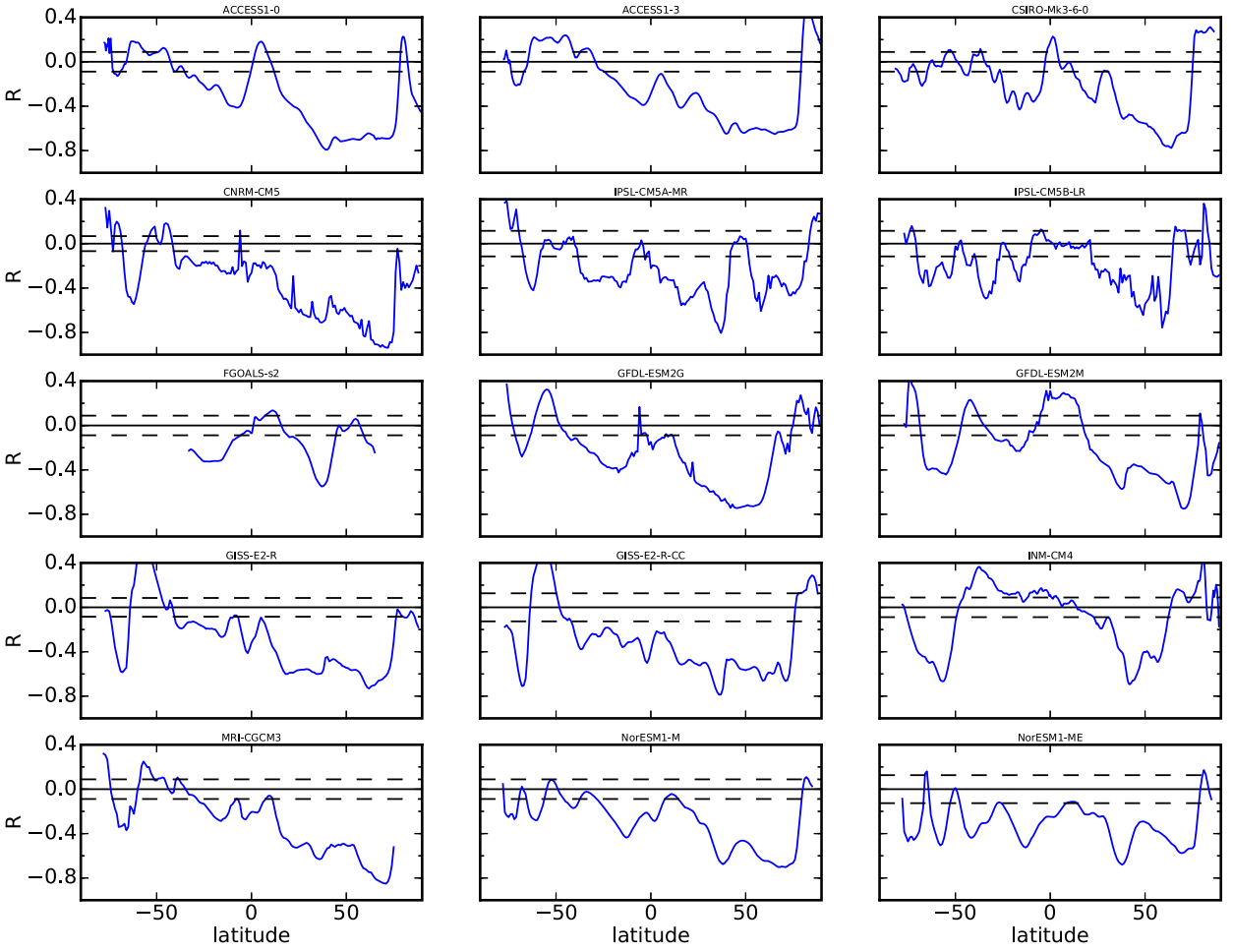

FIG. 3. Correlation between H_A and H_O as a function of latitude for the preindustrial control runs of the 15 CMIP5 models. The dashed lines show the 95% confidence level based on a *t* test.

each with a negative peak of over −6 PW. The heat transport in the ocean in the SH lies between −0.62 and −1.4 PW in all 15 models. These values for the SH heat transports in the CMIP5 models compare well to those estimated from reanalyses (Trenberth and Caron 2001) that found H_A reaching a negative peak of around −5 PW and an H_O negative peak of around −1 PW. There are a couple of anomalies worth noting with respect to H_O in the SH. FGOALS-s2 appears to have zero ocean heat transport south of 34°S. It remains unclear why this is the case, but most likely the data are unavailable below this latitude. All of the models (except for FGOALS-s2) show a peak in H_O at around 45°S; however, this peak becomes positive in 6 of the 15 models, indicating a net northward flow at this latitude. Trenberth and Caron (2001) also identified a peak at this latitude and demonstrated that this was a result of the net northward flow in the Atlantic Ocean, combined with a localized peak in the Indian Ocean. In summary, all 15 CMIP5 models are producing reasonable estimates of both H_A and H_O in the SH compared to reanalyses, though there is more spread between the models and an apparent issue with H_O in the SH in FGOALS-2s.

To confirm the presence of Bjerknes compensation, we calculate the correlations between the heat transports at each latitude (Fig. 3). In the NH, the CMIP5 models show low anticorrelation in the tropics where the BJC mechanism does not appear to be acting, stronger anticorrelations in the midlatitudes between approximately 40° and 70°N, and low anticorrelation or even small positive correlation between 75°N and at the pole where sea ice cover greatly limits air–sea interaction. FGOALS-s2 and IPSL-CM5A-MR are both anomalous in having a peak of positive or zero correlation at around 50°N. The broad pattern produced in the CMIP5 models is similar to that found in previous studies (Shaffrey and Sutton 2006; Jungclaus and Koenigk 2010; Outten and Esau 2017). Of the 15 CMIP5 models studied here, 14

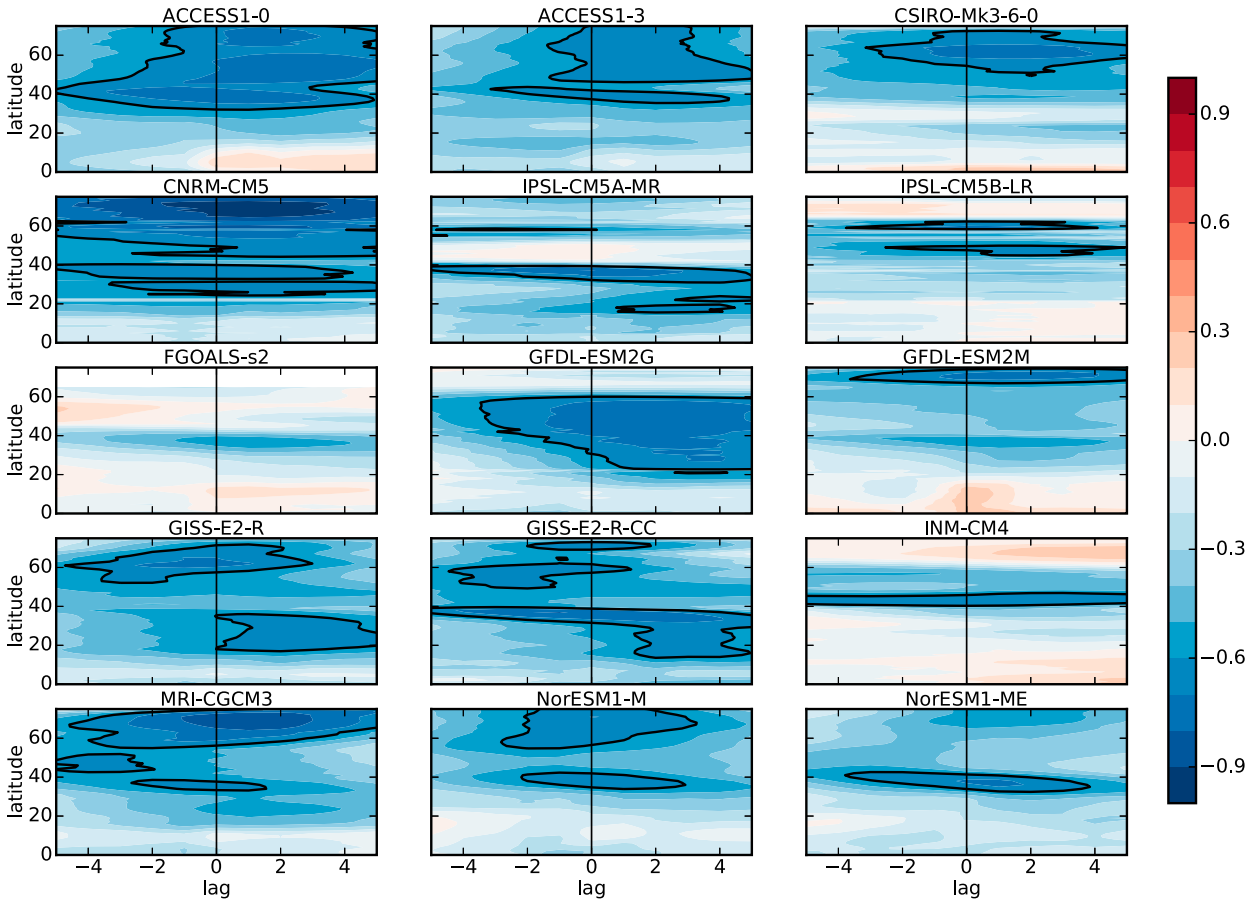

FIG. 4. Lag correlation in years between H_A and H_O as a function of latitude for the Northern Hemisphere for the preindustrial control runs. Positive lag indicates the ocean is leading the atmosphere, contours every $R = 0.1$. Vertical line indicates zero lag; bold line is the $R = -0.6$ contour.

show peaks of strong anticorrelation in the NH, with the magnitude of correlation of $|R| \geq 0.7$. This indicates that BJC is present in all of these models as anomalies in oceanic heat transport that are compensated for by anomalies in atmospheric heat transport and vice versa. The only model to not show such strong anticorrelation between the atmospheric and oceanic heat transports is FGOALS-s2, which peaks at only $R = -0.56$.

The strongest anticorrelation in the previous studies occurred at approximately 70°N, and through regression analysis, it was determined that this was related to the marginal ice zone (MIZ). The MIZ is important since it is an area where the decoupling of the atmosphere and ocean, caused by sea ice, breaks down. This allows warm ocean waters to meet with the cold Arctic air, which induces large air–sea fluxes and thus strong air–sea interaction. While many of the CMIP5 models do show the strongest anticorrelation at around 70°N, most models also show a second peak in anticorrelation located at approximately 45°N. This is the latitude at which storm tracks occur in both the Atlantic and Pacific Oceans, which are again areas of large air–sea fluxes and strong air–sea interaction. Far weaker midlatitude peaks of anticorrelation were previously found in HadCM3 (Shaffrey and Sutton 2006, their Fig. 2), and in ECHAM5 (Jungclaus and Koenigk 2010, their Fig. 3). Outten and Esau (2017) performed a regression analysis between the BJC signal and the surface heat fluxes over the Northern Hemisphere in the Bergen Climate Model (their Fig. 6). This analysis showed bands of positive and negative heat flux changes in the locations of the storm tracks in both the North Atlantic and North Pacific, suggesting a meridional shift in the North Atlantic and North Pacific storm tracks related to the phase of BJC in that model. While indications of a midlatitude peak in anticorrelation do exist in the past studies, Fig. 3 shows that the anticorrelation in the midlatitudes can be greater than the anticorrelation associated with the MIZ, as is the case in half of the models (e.g., NorESM1-ME).

TABLE 2. Maximum anticorrelation (minimum R) between H_A and H_O, along with the ocean lead (yr) and latitude at which it occurs for both the preindustrial control runs and historical runs of the 15 CMIP5 models. CSIRO Mk3.6.0 and FGOALS-s2 lacked the fields required to calculate BJC for the historical runs.

	Preindustrial control run			Historical run		
Model name	Min R	Lead–lag (yr)	Latitude (°N)	Min R	Lead–lag (yr)	Latitude (°N)
ACCESS1.0	−0.79	0	39.8	−0.81	−3	46.9
ACCESS1.3	−0.70	2	49.4	−0.88	1	58.1
CSIRO Mk3.6.0	−0.77	1	63.9	—	—	—
CNRM-CM5	−0.94	1	72.0	−0.93	1	72.0
IPSL-CM5A-MR	−0.80	0	37.0	−0.75	0	82.0
IPSL-CM5B-LR	−0.77	0	59.0	−0.61	−1	43.0
FGOALS-s2	−0.56	1	37.0	—	—	—
GFDL-ESM2G	−0.79	2	45.0	−0.87	4	57.0
GFDL-ESM2M	−0.75	1	71.0	−0.71	1	26.0
GISS-E2-R	−0.74	−1	62.0	−0.84	0	71.0
GISS-E2-R-CC	−0.80	−1	37.0	−0.90	1	72.0
INM-CM4.0	−0.70	0	42.0	−0.62	5	49.5
MRI-CGCM3	−0.87	1	70.0	−0.85	1	66.0
NorESM1-M	−0.70	0	71.0	−0.60	5	75.0
NorESM1-ME	−0.73	1	37.0	−0.75	0	72.0

Figure 3 also shows that in the SH, the compensation is small at most latitudes in the models. The exception is a peak of anticorrelations seen in a few of the models between 60° and 70°S [e.g., Goddard Institute for Space Studies Model E2, coupled with Russell and interactive terrestrial carbon cycle (GISS-E2-R-CC)]. This is again a region of MIZ, where the Southern Ocean meets the coast of Antarctica and the breakdown of decoupling between the warm ocean waters and cold Antarctic air allows for large air–sea fluxes. Since this is the only feature of interest in the SH and it does not occur in most of the models, the remainder of this study will focus on the NH, and investigation of BJC around the coast of Antarctica will be left for future studies.

Since the presence of BJC has been confirmed in the models, the next stage is to investigate the temporal variability of the atmospheric and oceanic heat transports. In HadCM3 and ECHAM5, variations in H_O were found to be leading variations in H_A by 1 year (Shaffrey and Sutton 2006; Jungclaus and Koenigk 2010), suggesting that the changes in ocean heat transport were driving changes in the atmospheric heat transport. However, this was not found to be the case in BCM (Outten and Esau 2017), when no lead or lag was identified between the variations in H_A and H_O. Here we performed lag correlations to identify both the latitude and the lead–lag between H_A and H_O at which the strongest anticorrelation was found in each of the 15 CMIP5 models (Fig. 4). The peak anticorrelation is given in Table 2 along with the latitude and lead–lag at which it occurred.

With the exception of FGOALS-s2, the CMIP5 models show a peak anticorrelation of between $R = -0.70$ and $R = -0.94$, indicating the presence of strong compensation in these models between H_A and H_O. Of the 15 models, 8 have the variations of H_O leading the variations in H_A by 1 or 2 years, suggesting that the ocean is driving the atmosphere in these models, while 5 of the models show no lead or lag. The two models from the NASA GISS both show the strongest compensation occurring when variations in atmospheric heat transport are leading the variations in oceanic heat transport by one year. These findings indicate that BJC may still be present whether the anomalies in H_O lead anomalies in H_A or not.

Four of the models have the prominent compensation occurring at around 70°N where the presence of the MIZ allows for strong air–sea interaction, as was previously found in HadCM3, ECHAM5, and BCM (Shaffrey and Sutton 2006; Jungclaus and Koenigk 2010; Outten and Esau 2017). While CSIRO Mk3.6.0 and GISS-E2-R show the strongest anticorrelation at around 63.9° and 62.0°N, respectively, these are both likely related to the presence of the MIZ in these models, since investigation revealed that both models have high sea ice extents in the Arctic region compared to observations. The remaining nine models have more prominent compensations in the midlatitudes between 37.0° and 59.0°N, latitudes that contain the storm tracks in both the North Atlantic and North Pacific.

The time series of heat transport anomalies in the atmosphere and ocean at the latitude and lag of strongest anticorrelation is shown in Fig. 5. These plots are limited to the first 250 years of the preindustrial control runs for the benefit of clarity and comparability; however, the heat transport anomalies over the full preindustrial

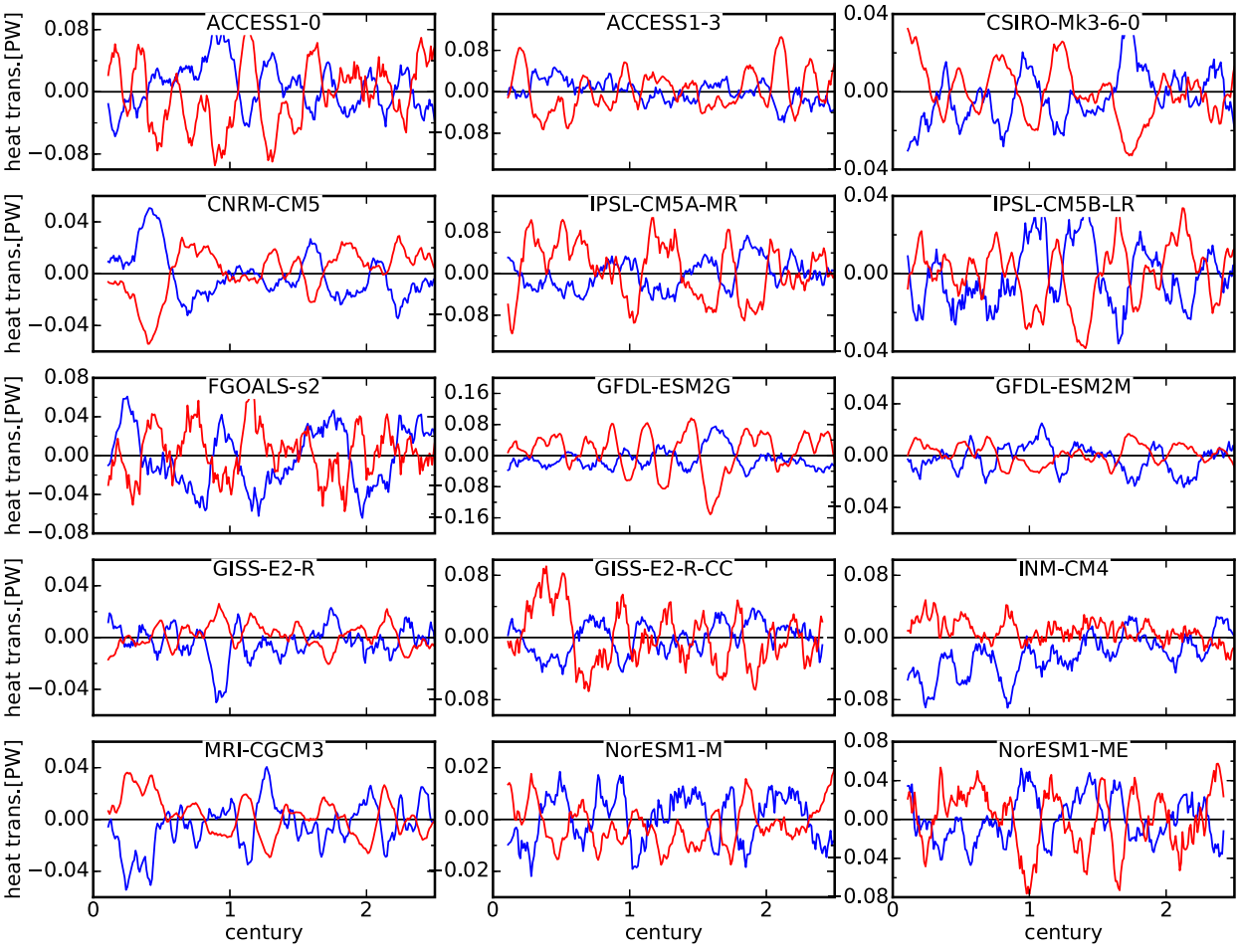

FIG. 5. Anomalies in atmospheric (blue) and oceanic (red) heat transport at the latitude and lag of highest compensation for the first 250 years of the preindustrial control runs, as given in Table 2. Note that each panel has an independent y axis.

control runs in the models are broadly similar (Fig. S2). The anticorrelation indicative of the presence of BJC is visible in all of the time series as the heat transport anomalies transition from periods of positive H_A balanced by negative H_O to periods of negative H_A balanced by positive H_O. The difference in magnitudes in these time series is directly related to their respective latitudes, since the atmosphere and ocean both have higher transports in the midlatitudes than at the high latitudes. Despite these differences in magnitude, the anomalies of heat transport are approximately balanced in all models. For example, in the ACCESS1.0 model, the peak occurs at around 40°N, where the atmosphere and ocean are transporting 4.4 and 0.9 PW, respectively. From Fig. 5, the anomalies in both H_A and H_O in the ACCESS1.0 model are around ± 0.05 PW or $\pm 1\%$ of the total H_A at this latitude and $\pm 5\%$ of the total H_O. Similarly, in NorESM1-M, the peak occurs around 70°N, where the model is only transporting 1.7 PW in the atmosphere and 0.2 PW in the ocean. Again from Fig. 5, the anomalies are approximately ± 0.02 PW or around $\pm 1\%$ of the total H_A and $\pm 10\%$ of the total H_O. This consistent balance in the anomalies of heat transport irrespective of the latitude and thus magnitude of the total heat transport further supports the conclusion that the anomalies in heat transport in the atmosphere and ocean are compensating for one another through Bjerknes compensation.

The variations in the models appear to be semiregular as the heat transport anomalies change from being dominated by H_A to being dominated by H_O. The average amount of time the models spend in this preferred state, with the anomalies in the atmosphere and ocean partially or fully compensating for one another, is 78%. There are very few years in any model where the H_A and H_O anomalies are in unison with one another, that is, both positive or both negative. The semiregular variability is suggestive of a multidecadal oscillation in each

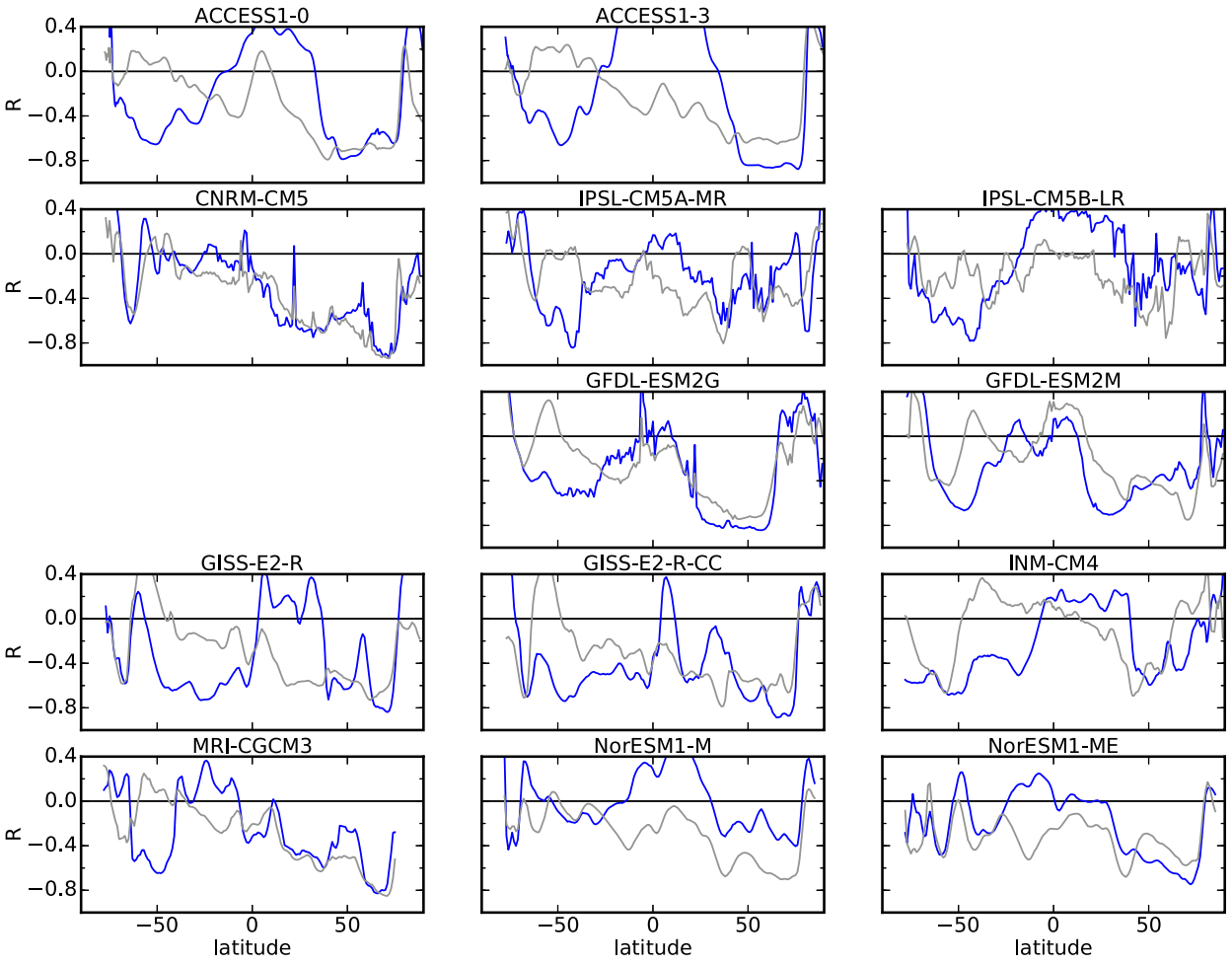

FIG. 6. Correlation between the H_A and H_O as a function of latitude for the historical run (blue), compared to the preindustrial control runs (gray), in the 13 of 15 CMIP5 models for which the heat transports could be calculated in the historical runs.

of the models. However, while fast Fourier transform analysis on the H_A anomalies did show that most of the models had a peak in frequency in the range of 40–70 years, in most cases, this peak was not distinct from the noise. It can be seen from the time series of heat transport anomalies that the time spent in either the atmosphere positive state or the ocean positive state is highly variable, even within each individual model. This raises the question of whether the variations in heat transports found in the CMIP5 models are the result of a multidecadal oscillation or if they are simply red noise in nature. Addressing this question is beyond the scope of the current study and will be the focus of future work.

One anomalous feature that does stand out in Fig. 5 is the steady trend seen in INM-CM4.0. There is a positive trend in H_A and negative trend in H_O over the entire 500 years of the preindustrial control run in this model. This may suggest that the spinup period for the model was insufficiently long for the model to reach a stable state. The other 14 models, however, have no apparent trend in their heat transport anomalies.

4. BJC in CMIP5 historical runs

The total meridional atmospheric and oceanic heat transports were calculated for the historical runs of 13 of the 15 CMIP5 models, all covering the period of 1850–2005. The two missing models are FGOALS-s2, for which the historical simulation was retracted from the CMIP5 archive, and the CSIRO Mk3.6.0 model, which lacks the fields required to calculate ocean heat transport. The mean heat transports as a function of latitude are very similar to those seen in the preindustrial control runs, with maxima and minima in H_A of around ±4–5 PW at 40°N and 40°S, respectively; NH peaks in H_O of approximately 1–2 PW around 20°N; and broad SH negative peak H_O of approximately half this magnitude located between 20° and 40°S.

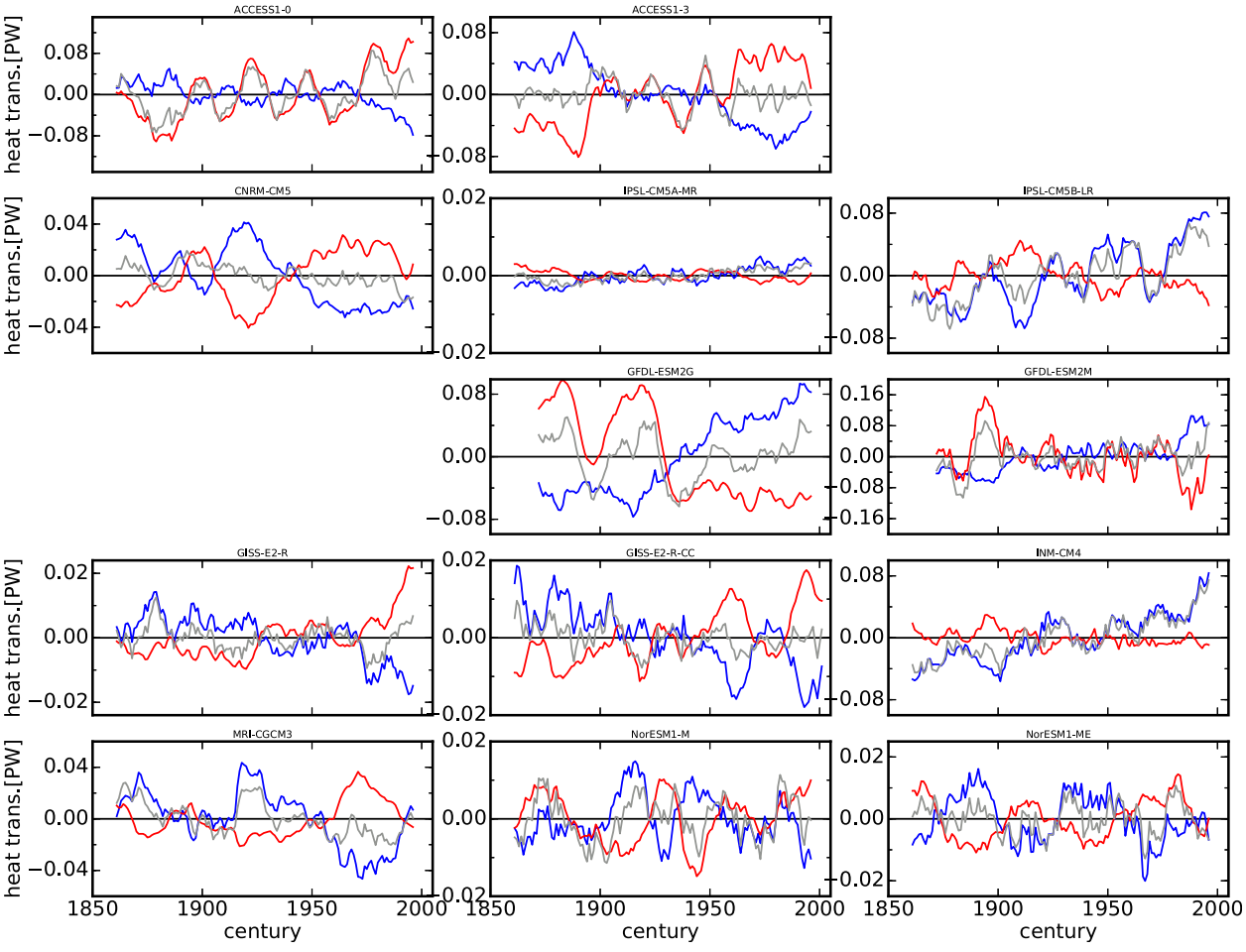

FIG. 7. Anomalies in atmospheric (blue), oceanic (red), and total (gray) heat transport at the latitude and lag of highest compensation for the historical runs, as given in Table 2. Note that each panel has an independent y axis.

The correlation between H_A and H_O anomalies as a function of latitude for the historical runs is shown in Fig. 6, along with the correlation from the preindustrial control runs for comparison. The correlations are very similar between the control and historical runs in the extratropical NH in all of the models. The peaks in anticorrelation are located at the same latitudes as in the preindustrial control runs in most of the models, and all models have peaks in anticorrelation in excess of $R = -0.6$, 10 of which still peak in excess of $R = -0.7$. This indicates that despite the addition of external forcings, including volcanic emissions, anthropogenic greenhouse gases, and tropospheric aerosols, BJC is still present in the extratropical NH. Vellinga and Wu (2008) also found in their model experiments that partial compensation could occur in the presence of considerable TOA changes. While in the tropics a few of the models remain broadly unchanged (e.g., CNRM-CM5), others show large positive correlations (e.g., ACCESS1.0, ACCESS1.3, and GISS-E2-R). Most of the models also show large differences in the SH correlations as well, although the peaks of anticorrelation between 60° and 70°S are still present. These results indicate that BJC breaks down in the tropics and midlatitude SH in the historical runs, while still being present at the locations where it was strongest in the preindustrial control runs, that is, the MIZ in the NH and SH and in the presence of the NH storm tracks. This suggests that the multidecadal variability associated with BJC should play a role in determining heat transports in these locations in current real-world observations. Previous studies have shown that this variability associated with BJC at high latitudes in the NH can induce changes in the air–sea fluxes, leading to changes in surface air temperature and in turn changing mean sea level pressure and even geopotential heights over large areas of the extratropical NH (Outten and Esau 2017; Jungclaus and Koenigk 2010). The problem with detecting BJC in the real world is the lack of

observations, both in time and in space, especially in the ocean. Some attempts have been made to identify BJC in paleo-reconstructions of temperature, but these have so far been hindered by the temporal resolution and uncertainties associated with such datasets. If such problems were to be overcome, BJC would be a valuable tool in assessing the decadal predictability in these regions.

Lag correlations were again used to identify the latitude and lead–lag of the strongest anticorrelation in the historical runs of the models (Fig. S3). All of the models still show a strong anticorrelation indicative of the presence of BJC. However, in IPSL-CM5B-LR, INM-CM4.0, and NorESM1-M this anticorrelation is only around $R = -0.61$, while in the remaining 10 models, the anticorrelation is greater than $|R| \geq 0.7$, with CNRM-CM5 having the strongest anticorrelation at $R = -0.93$ (Table 2). Examining the time series of H_A and H_O anomalies at the latitude and lag of strongest anticorrelation (Fig. 7), it is again found that the anomalies in H_A compared to H_O in each model are of similar magnitude, irrespective of the latitude they occur at, further supporting the idea of compensation between the H_A and H_O anomalies. The latitudes with the strongest anticorrelation have changed in many of the models, although the models can still be separated into those with the most prominent compensation occurring in the extratropical midlatitudes where there are strong air–sea fluxes located in the regions of storm tracks, or those with the most prominent compensation occurring at high latitudes where the MIZ is located. Of particular note is IPSL-CM5A-MR that has very small anomalies in heat transport in Fig. 7. The peak anticorrelation in this model occurs at 82°N, at which latitude the atmosphere and ocean transport only 0.29 and −0.005 PW, respectively, hence the small magnitude of the heat transport anomalies. While IPSL-CM5A-MR does have consistently low summer sea ice extent compared to the other models, which may partially explain why the peak anticorrelation is located so far north, we also note that the model has a second peak of similar magnitude ($R = -0.66$ vs $R = -0.69$) located at 40°N, the same latitude as the peak anticorrelation in the preindustrial control run (Fig. 6).

The lead–lag at which the compensation is strongest has also changed in the models. While nine of the models still show a lead or lag of 1 year, GFDL-ESM2G, INM-CM4.0, and NorESM1-M all show H_O leading H_A by 4 or 5 years, while in the ACCESS1.0 model, H_A is leading H_O by 3 years. Many of the models also show a trend in the heat transport anomalies over the historical period, as calculated using linear regression ($p \leq 0.01$). ACCESS1.0, ACCESS1.3, CNRM-CM5, GISS-E2-R, GISS-E2-R-CC, and MRI-CGCM3 all have positive trends in H_O and negative trends in H_A, while IPSL-CM5A-MR, IPSL-CM5B-LR, GFDL-ESM2G, GFDL-ESM2M, and INM-CM4.0 show the reverse, with negative trends in H_O and positive trends in H_A. The two NorESM models both show no significant trend in either H_A or H_O anomalies. These trends appear to be unrelated to specific local factors, for example, sea ice retreat, since different models have opposing trends at the same latitudes; for example, ACCESS1.3 and GFDL-ESM2G both have peak anticorrelation around 57°–58°N, and yet one model shows a positive H_A trend, while the other shows a positive H_O trend. Since the high latitudes have warmed faster than the mid- and low latitudes in the NH over the historical period, these findings indicate that in response to a decreased meridional temperature gradient and/or increased temperatures at the latitudes of strongest anticorrelation, the CMIP5 models have either increased in atmospheric heat transport, for example, through increased latent heat flux, or increased in oceanic heat transport. While it remains unclear why the models respond in one way or the other, it does appear to be related to the specific physics or dynamics in those models, since all pairs of different versions of the same model have the same response, that is, both ACCESS models have H_A and H_O trends of the same sign, as do both IPSL models, both GFDL models, both GISS models, and even both NorESM models, which have no significant trend. Examining the future projection runs of the CMIP5 models, driven by various representative concentration pathway scenarios, would give some insight into how these trends will change in the models and will be undertaken in future work.

5. Discussion

The original hypothesis of Bjerknes (1964) required that the top-of-atmosphere radiation fluxes remain approximately constant so that the total heat being transported around the climate system remains approximately constant. Under anthropogenic climate change, the climate system has warmed over the past 150 years, and this condition may not necessarily hold. However, the results presented in the previous section demonstrate that even under the condition of a warming world, Bjerknes compensation is still present as anomalies of heat transport in the atmosphere and ocean continue to counteract one another. In another recent study, BJC was identified in a 22 000-yr-long transient climate model simulation from the Last Glacial Maximum to preindustrial times (Yang et al. 2015b). In this simulation, it was found that the global total meridional heat transport changed little despite quite large and abrupt changes in Earth's temperature and ocean circulations. Yang et al. (2015b) identified that the small fluctuation in total global meridional heat transport was the result of compensating changes in the atmospheric

and oceanic heat transports, that is, BJC. This highlights the role of BJC as a fundamental property of the climate system.

A recent theoretical study investigated the mechanism underlying BJC by using a one-dimensional (1D) energy balance model (EBM) applied to a sphere and examining the response of atmospheric heat transport to perturbations of ocean heat transport (Liu et al. 2016). They defined a BJC ratio as $C = H_A/H_O$. In the 1D EBM, the atmospheric and oceanic heat transport anomalies always compensate for one another to a varying degree, that is, the ratio C is always negative, as H_A and H_O anomalies are always of opposite sign. In the CMIP5 models, the anomalies are of opposite sign approximately 75%–90% of the time in both the preindustrial control and historical runs of all models at the latitude and lag of greatest anticorrelation (Figs. 5, 7). Liu et al. (2016) suggested that a poleward perturbation of the ocean heat transport would induce extratropical warming and tropical cooling; however, with negative feedback everywhere in their model, these temperature anomalies were damped through top-of-atmosphere radiation. The temperature anomalies induced increased atmospheric heat transport toward the tropics, but because of the damping, the atmospheric heat transport always undercompensated for the ocean perturbation, resulting in a ratio with magnitude less than one. If the climate feedback was positive in some localized regions, as it often is in the tropics because of water vapor and cloud feedbacks (Zhang et al. 1994; Roe et al. 2015; Zelinka and Hartmann 2012), then the atmosphere should overcompensate for the ocean and the magnitude of the ratio will be greater than one. However, the CMIP5 models show little to no compensation in the tropics or the midlatitude SH, which is in agreement with Shaffrey and Sutton (2006), who suggest that BJC is not an appropriate model for the tropics.

When the one-dimensional EBM has negative feedback everywhere, all latitudes have a constant ratio of $C \approx -0.7$. However, when the tropical region of the EBM has a positive feedback applied, overcompensation is produced in the tropics, and the ratio smoothly decreases from the tropical boundary to the pole. While this broadly holds for the fully coupled GCMs studied here, they also show sharp variations at different latitudes where the compensation between anomalies of H_A and H_O varies based on the physical processes at those locations (Fig. 6). Liu et al. (2016) suggest that a ratio of between $C = -0.7$ and $C = -0.8$ is seen in GCM studies with forced ocean heat transports, though stipulate that there is a large spread between different models. Since BJC is not present at many latitudes in the CMIP5 models, for example, midlatitude SH and tropics, we examine the BJC ratio only at the latitude and lag of highest anticorrelation (Table 3). In the preindustrial control runs, the mean ratio is $\overline{C} = -0.78$ with a standard deviation of $\sigma = 0.35$, which broadly agrees with the suggestion of Liu et al. (2016). INM-CM4.0, MRI-CGCM3, and NorESM1-M, however, all have ratios of magnitude greater than one, suggesting that at the locations of greatest anticorrelation, there is positive climate feedback. This can be seen directly in Fig. 5, where the magnitudes of the H_O anomalies are generally slightly larger than the anomalies of H_A. When external varying forcings are included, as in the historical runs, the situation changes. Approximately half the models show undercompensation of the ocean by the atmosphere, while the other half show overcompensation. The spread in ratio between the models also increases as indicated by the standard deviation of $\sigma = 0.50$. The greatest undercompensation is found in the ACCESS1.0 model, while the greatest overcompensation is found in the INM-CM4.0, and again this can been seen directly in the plot of H_A and H_O anomalies (Fig. 7). An alternative measure was the BJC rate, defined as the ratio of the standard deviations in H_A and H_O scaled by their correlation (Zhao et al. 2016). The values of this parameter are also given for the CMIP5 models in Table 3 and show consistently similar values to the BJC ratio, thus leaving the conclusions unchanged. These results indicate that in the preindustrial control runs, the strongest BJC mostly occurs in locations of negative climate feedback, but in the historical runs where external varying forcings are

TABLE 3. Median BJC ratio and the BJC rate at the latitude and lag of highest compensation in the preindustrial control and historical runs of the CMIP5 models with the mean and standard deviation across the models.

	Preindustrial control run		Historical run	
Model name	BJC ratio	BJC rate	BJC ratio	BJC rate
ACCESS1.0	−0.63	−0.59	−0.31	−0.36
ACCESS1.3	−0.42	−0.40	−0.82	−0.84
CSIRO Mk3.6.0	−0.74	−0.80	—	—
CNRM-CM5	−0.92	−0.93	−1.08	−1.05
IPSL-CM5A-MR	−0.44	−0.41	−1.25	−1.32
IPSL-CM5B-LR	−0.87	−0.80	−1.52	−1.38
FGOALS-s2	−0.68	−0.63	—	—
GFDL-ESM2G	−0.39	−0.37	−0.79	−0.75
GFDL-ESM2M	−0.85	−0.85	−0.46	−0.53
GISS-E2-R	−0.81	−0.89	−0.98	−0.89
GISS-E2-R-CC	−0.46	−0.44	−1.02	−1.03
INM-CM4.0	−1.84	−1.54	−2.37	−1.99
MRI-CGCM3	−1.08	−1.10	−1.12	−1.35
NorESM1-M	−1.03	−0.81	−0.46	−0.58
NorESM1-ME	−0.60	−0.055	−0.85	−0.89
Mean ratio	−0.78	−0.74	−1.02	−1.01
Standard deviation	0.35	0.30	0.50	0.40

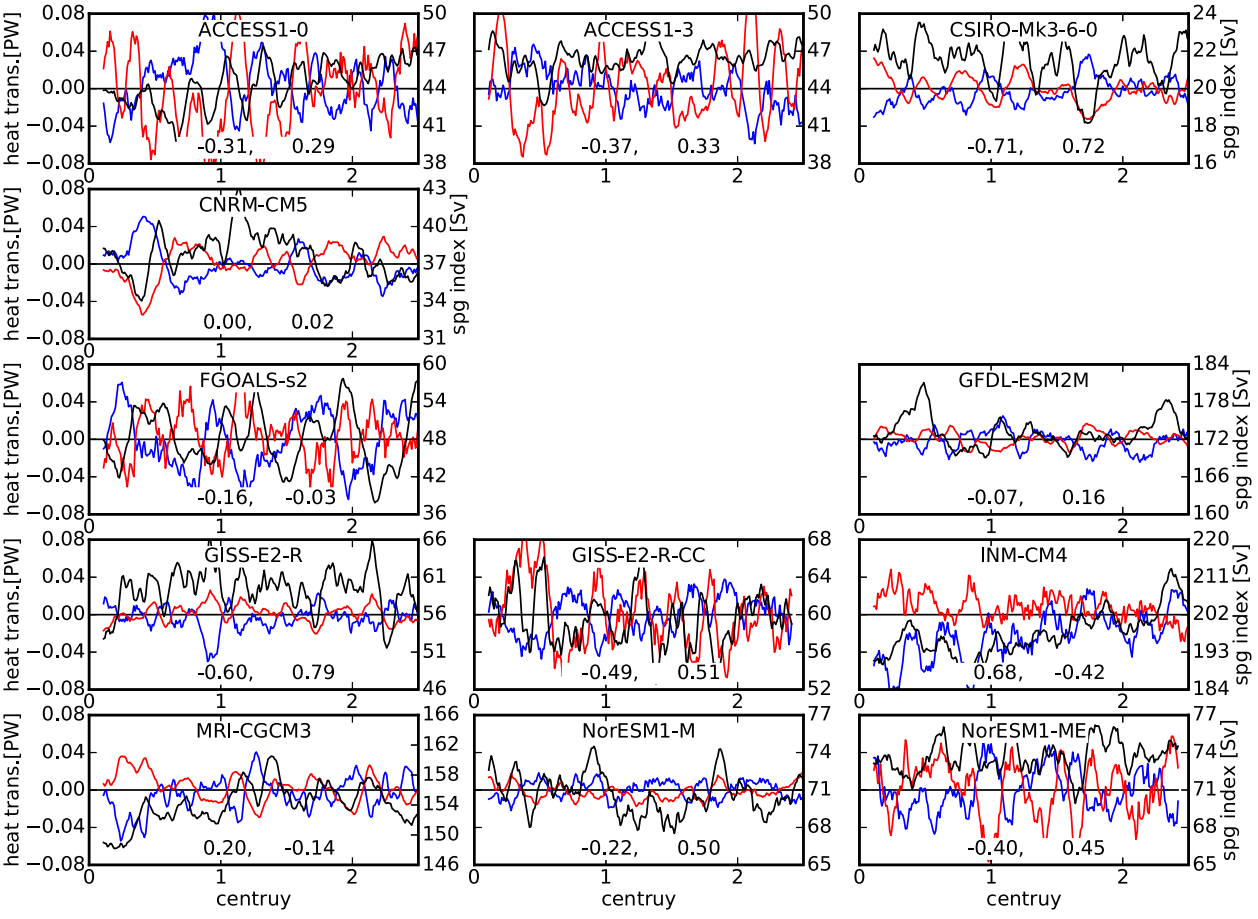

FIG. 8. Anomalies in atmospheric (blue) and oceanic (red) heat transport at the latitude and lag of highest compensation compared to the variations in the strength of the subpolar gyre (black) in the first 250 years of the preindustrial control runs of 12 CMIP5 models. The correlations between the SPGI and the atmospheric (left value) and oceanic (right value) heat transports are given at the bottom of each panel.

included, the strongest BJC can occur in locations with either negative or positive climate feedback. Further work is currently underway to investigate the role of climate feedbacks in shaping BJC in the presence of external forcing.

In a previous study of Bjerknes compensation in the Bergen Climate Model, the variability of the strength of the subpolar gyre was strongly correlated to the anomalies of atmospheric heat transport, but not to the anomalies of ocean heat transport (Outten and Esau 2017). This suggested the possibility that the subpolar gyre was spun up or spun down by changes in the surface winds, which varied with changing eddy heat transport in the atmosphere. To investigate this possibility, H_A and H_O were compared to the subpolar gyre index (SPGI) for 12 of the CMIP5 models in this study. The two IPSL models and GFDL-ESM2G lacked the fields required to calculate the SPGI. As in Outten and Esau (2017), the SPGI was created by taking the absolute value of the local minimum of the depth-integrated streamfunction in the subpolar North Atlantic for each of the CMIP5 models.

In 10 of the 12 models, the SPGI is negatively correlated with H_A and positively correlated with H_O (Fig. 8; Fig. S4), as expected. The two exceptions are MRI-CGCM3, which shows very weak correlations to both H_A and H_O, and INM-CM4.0, which is dominated by a long-term trend throughout the preindustrial control run, as noted previously. While eight of the models show reasonable correlations with H_A and H_O, lying between $R = -0.35$ and $R = 0.83$ over the full model runs, four of the models show weak, or even nonsignificant, correlations in both H_A and H_O. Most importantly, in each of the 12 models, the correlations between the SPGI and H_A or H_O are comparable over the full model runs. This indicates that the findings in the Bergen Climate Model of the strength of the subpolar gyre being strongly tied to the changes in H_A but not H_O are unique to that model,

and possibly even to that simulation. However, it should be noted that the Bergen Climate Model has been shown to have a quite realistic reproduction of the North Atlantic Current, the shape of the subpolar gyre, and the water mass transformation in the subpolar gyre region when compared to other CMIP models (Langehaug et al. 2012). An investigation of the shape of the subpolar gyre in the CMIP5 models shows no discernable pattern between the shape of the gyre and its relationship to H_A and H_O. While the correlations here demonstrate that the strength of the subpolar gyre does vary with changes in the heat transports in the atmosphere and ocean, it does not appear to be indicative of a mechanism where the atmosphere feeds back into the ocean on multidecadal time scales.

6. Conclusions

A systematic compensation of northward heat transport anomalies between the atmosphere and ocean has been found in 15 CMIP5 models. Previous studies have confirmed the presence of BJC in three climate models—HadCM3, ECHAM5, and BCM—but the results of this study strongly support the idea that BJC is a mechanism present in many if not all global climate models to varying degrees. It should be noted that because of the required fields not being available in many models, this study has only examined BJC in a subset of the CMIP5 models, and that a number of the CMIP5 models share the same or similar components and thus are not truly independent from one another.

While previous studies of BJC in the absence of external forcing have all found the most prominent compensation to occur where the warm ocean meets the cold Arctic atmosphere, this study has shown that a second often dominant peak in compensation occurs in many models at the latitude of the midlatitude storm tracks, a region that is known for its strong air–sea interactions. It has also been shown that in the absence of external forcings, the variations in the ocean heat transport lead the heat transport variations in the atmosphere in approximately half of the models included in this study.

In the presence of external forcings, such as in the CMIP5 historical simulations, BJC continues to be present, despite the possibility that such forcing may violate the conditions for BJC as proposed by Bjerknes (1964). In these simulations, many of the models show a clear trend in the heat transports, with some models showing positive trends in H_A and negative trends in H_O and others showing the reverse. This suggests that in each model the heat transport in either the atmosphere or ocean will increase in response to the external forcing. It is interesting to note that every pair of the same model shows the trends in H_A and H_O to be of the same sign; for example, both ACCESS models show a positive trend in H_O and a negative trend in H_A, both GFDL models negative trends in H_O and positive trends in H_A. While this could suggest that it is a property of the mode physics that determines whether it is the atmospheric or oceanic heat transport that increases in response to the external forcing, this could also be a result of the initial conditions for the simulations. Further investigation would be required to identify what factor is determining this and potentially to identify whether the atmospheric or oceanic heat transports are increasing or decreasing in response to the current warming.

The physical mechanism underlying the multidecadal variability associated with Bjerknes compensation remains unclear, and while many groups are already studying this issue, the identification of BJC in multiple CMIP5 models provides an excellent resource for such investigations. Given the importance of meridional heat transport in the ocean and the complexities of accurately calculating it from the various ocean model grids, we would propose that the hfbasin field should be made a high-priority variable for future phases of the Coupled Model Intercomparison Project.

Acknowledgments. This work was funded by the MEDEVAC and BECOMEGYRE projects funded by the Bjerknes Centre for Climate Research (BCCR). We acknowledge the World Climate Research Programme's Working Group on Coupled Modelling, which is responsible for CMIP, and we thank the climate modeling groups (listed in Table 1 of this paper) for producing and making available their model output. For CMIP, the U.S. Department of Energy's Program for Climate Model Diagnosis and Intercomparison provides coordinating support and led development of software infrastructure in partnership with the Global Organization for Earth System Science Portals.

REFERENCES

Bishop, S. P., F. O. Bryan, and R. J. Small, 2015: Bjerknes-like compensation in the wintertime North Pacific. *J. Phys. Oceanogr.*, **45**, 1339–1355, https://doi.org/10.1175/JPO-D-14-0157.1.

Bjerknes, J., 1964: Atlantic air-sea interaction. *Advances in Geophysics*, Vol. 10, Academic Press, 1–82, https://doi.org/10.1016/S0065-2687(08)60005-9.

Farneti, R., and G. K. Vallis, 2013: Meridional energy transport in the coupled atmosphere–ocean system: Compensation and partitioning. *J. Climate*, **26**, 7151–7166, https://doi.org/10.1175/JCLI-D-12-00133.1.

Held, I. M., 2001: The partitioning of the poleward energy transport between the tropical ocean and atmosphere. *J. Atmos. Sci.*, **58**, 943–948, https://doi.org/10.1175/1520-0469(2001)058<0943:TPOTPE>2.0.CO;2.

Huber, M. B., and L. Zanna, 2017: Drivers of uncertainty in simulated ocean circulation and heat uptake. *Geophys. Res. Lett.*, **44**, 1402–1413, https://doi.org/10.1002/2016GL071587.

Jacob, R. L., 1997: Low frequency variability in a simulated atmosphere-ocean system. Ph.D. dissertation, University of Wisconsin–Madison, 155 pp.

Jungclaus, J. H., and T. Koenigk, 2010: Low-frequency variability of the Arctic climate: The role of oceanic and atmospheric heat transport variations. *Climate Dyn.*, **34**, 265–279, https://doi.org/10.1007/s00382-009-0569-9.

Langehaug, H. R., I. Medhaug, T. Eldevik, and O. H. Otterå, 2012: Arctic/Atlantic exchanges via the subpolar gyre. *J. Climate*, **25**, 2421–2439, https://doi.org/10.1175/JCLI-D-11-00085.1.

Liu, Z., H. Yang, C. He, and Y. Zhao, 2016: A theory for Bjerknes compensation: The role of climate feedback. *J. Climate*, **29**, 191–208, https://doi.org/10.1175/JCLI-D-15-0227.1.

Myhre, G., and Coauthors, 2013: Anthropogenic and natural radiative forcing. *Climate Change 2013: The Physical Science Basis*, T. F. Stocker et al., Eds., Cambridge University Press, 659–740, http://www.ipcc.ch/pdf/assessment-report/ar5/wg1/WG1AR5_Chapter08_FINAL.pdf.

Outten, S., and I. Esau, 2017: Bjerknes compensation in the Bergen Climate Model. *Climate Dyn.*, **49**, 2249–2260, https://doi.org/10.1007/s00382-016-3447-2.

Roe, G. H., N. Feldl, K. C. Armour, Y.-T. Hwang, and D. M. W. Frierson, 2015: The remote impacts of climate feedbacks on regional climate predictability. *Nat. Geosci.*, **8**, 135–139, https://doi.org/10.1038/ngeo2346.

Shaffrey, L., and R. Sutton, 2004: The interannual variability of energy transports within and over the Atlantic Ocean in a coupled climate model. *J. Climate*, **17**, 1433–1448, https://doi.org/10.1175/1520-0442(2004)017<1433:TIVOET>2.0.CO;2.

——, and ——, 2006: Bjerknes compensation and the decadal variability of energy transports in a coupled climate model. *J. Climate*, **19**, 1167–1181, https://doi.org/10.1175/JCLI3652.1.

Trenberth, K. E., and J. M. Caron, 2001: Estimates of meridional atmosphere and ocean heat transports. *J. Climate*, **14**, 3433–3443, https://doi.org/10.1175/1520-0442(2001)014<3433:EOMAAO>2.0.CO;2.

Van der Swaluw, E., S. S. Drijfhout, and W. Hazeleger, 2007: Bjerknes compensation at high northern latitudes: The ocean forcing the atmosphere. *J. Climate*, **20**, 6023–6032, https://doi.org/10.1175/2007JCLI1562.1.

Vellinga, M., and P. Wu, 2008: Relations between northward ocean and atmosphere energy transported in a coupled climate model. *J. Climate*, **21**, 561–575, https://doi.org/10.1175/2007JCLI1754.1.

Yang, H., Y. Wang, and Z. Liu, 2013: A modelling study of the Bjerknes compensation in the meridional heat transport in a freshening ocean. *Tellus*, **65A**, 18480, https://doi.org/10.3402/tellusa.v65i0.18480.

——, Q. Li, K. Wang, Y. Sun, and D. Sun, 2015a: Decomposing the meridional heat transport in the climate system. *Climate Dyn.*, **44**, 2751–2768, https://doi.org/10.1007/s00382-014-2380-5.

——, Y. Zhao, Z. Liu, Q. Li, F. He, and Q. Zhang, 2015b: Heat transport compensation in atmosphere and ocean over the past 22,000 years. *Sci. Rep.*, **5**, 16661, https://doi.org/10.1038/srep16661.

——, ——, and ——, 2016: Understanding Bjerknes compensation in atmosphere and ocean heat transports using a coupled box model. *J. Climate*, **29**, 2145–2160, https://doi.org/10.1175/JCLI-D-15-0281.1.

Zelinka, M. D., and D. L. Hartmann, 2012: Climate feedbacks and their implications for poleward energy flux changes in a warming climate. *J. Climate*, **25**, 608–624, https://doi.org/10.1175/JCLI-D-11-00096.1.

Zhang, M. H., J. J. Hack, J. T. Kiehl, and R. D. Cess, 1994: Diagnostic study of climate feedback processes in atmospheric general circulation models. *J. Geophys. Res.*, **99**, 5525–5537, https://doi.org/10.1029/93JD03523.

Zhao, Y., H. Yang, and Z. Liu, 2016: Assessing Bjerknes compensation for climate variability and its time-scale dependence. *J. Climate*, **29**, 5501–5512, https://doi.org/10.1175/JCLI-D-15-0883.1.